HHS Public Access

Author manuscript

J Mol Biol. Author manuscript; available in PMC 2017 February 27.

Published in final edited form as:

J Mol Biol. 2016 February 27; 428(5 Pt A): 822–833. doi:10.1016/j.jmb.2015.08.021.

N6-methyladenosine modification in a long non-coding RNA hairpin predisposes its conformation to protein binding

Katherine I. Zhou[1], **Marc Parisien**[2], **Qing Dai**[3], **Nian Liu**[3], **Luda Diatchenko**[2], **Joseph R. Sachleben**[4], and **Tao Pan**[5,6,*]

[1]Medical Scientist Training Program, The University of Chicago, Chicago, Illinois 60637, USA

[2]The Alan Edwards Centre for Research on Pain, McGill University, Montréal, Québec H3A 0G4, Canada

[3]Department of Chemistry, The University of Chicago, Chicago, Illinois 60637, USA

[4]Biomolecular NMR Core Facility, Biological Sciences Division, The University of Chicago, Chicago, Illinois 60637, USA

[5]Department of Biochemistry and Molecular Biology, The University of Chicago, Chicago, Illinois 60637, USA

[6]Institute of Biophysical Dynamics, The University of Chicago, Chicago, Illinois 60637, USA

Abstract

N6-methyladenosine (m^6A) is a reversible and abundant internal modification of messenger RNA (mRNA) and long noncoding RNA (lncRNA) with roles in RNA processing, transport, and stability. Although m^6A does not preclude Watson-Crick base pairing, the *N6*-methyl group alters the stability of RNA secondary structure. Since changes in RNA structure can affect diverse cellular processes, the influence of m^6A on mRNA and lncRNA structure has the potential to be an important mechanism for m^6A function in the cell. Indeed, an m^6A site in the lncRNA metastasis associated lung adenocarcinoma transcript 1 (MALAT1) was recently shown to induce a local change in structure that increases the accessibility of a U_5-tract for recognition and binding by heterogeneous nuclear ribonucleoprotein C (HNRNPC). This m^6A-dependent regulation of protein binding through a change in RNA structure, termed 'm^6A-switch,' affects transcriptome-wide mRNA abundance and alternative splicing. To further characterize this first example of an m^6A-switch in a cellular RNA, we used nuclear magnetic resonance (NMR) and Förster resonance energy transfer (FRET) to demonstrate the effect of m^6A on a 32-nucleotide RNA hairpin derived from the m^6A-switch in MALAT1. The observed imino proton NMR resonances and FRET efficiencies suggest that m^6A selectively destabilizes the portion of the hairpin-stem where the U_5-tract is located, increasing the solvent accessibility of the neighboring bases while maintaining the overall hairpin structure. The m^6A-modified hairpin has a predisposed conformation that resembles the hairpin conformation in the RNA–HNRNPC complex more closely than the

*corresponding author: taopan@uchicago.edu.

unmodified hairpin. The m^{6}A-induced structural changes in the MALAT1 hairpin can serve as a model for a large family of m^{6}A-switches that mediate the influence of m^{6}A on cellular processes.

Graphical abstract

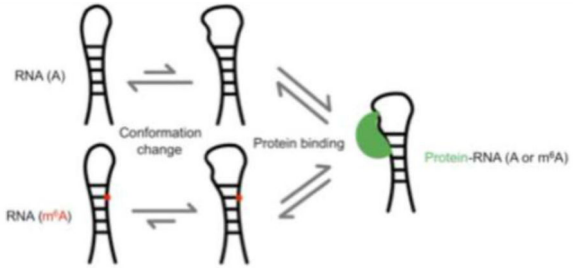

Keywords

N6-methyladenosine (m^{6}A); MALAT1 lncRNA; FRET; NMR; RNA structural modeling

Introduction

RNA modifications are important modulators of the structure and function of cellular RNAs. While the numerous modifications found in transfer RNA (tRNA) and ribosomal RNA (rRNA) have been extensively studied, much less is known about the function of the comparatively sparse modifications found in mRNA and lncRNA. Three types of internal mRNA and lncRNA modifications have been identified in higher eukaryotes so far [1–6]. Of these, *N6*-methyladenosine (m^{6}A) is the most abundant, with more than 12,000 m^{6}A sites in over 7,000 genes in the human transcriptome [2–4,7]. A reversible modification, m^{6}A occurs within RRm^{6}ACH motifs (R=A/G, H=A/C/U), with a high density of m^{6}A sites near stop codons and in long internal exons [3,4]. The m^{6}A methyltransferase complex is composed of the proteins methyltransferase-like 3 (METTL3), METTL14, and Wilms tumor 1 associated protein (WTAP) [8,9]. Two known demethylases, fat mass and obesity associated protein (FTO) and AlkB family member 5 (ALKBH5), are responsible for removing m^{6}A modifications [10,11]. Perturbations to these enzymes lead to altered m^{6}A levels and affect diverse processes including metabolism, spermatogenesis, the circadian clock, and stem cell differentiation [10–15].

m^{6}A modification has functional roles in RNA splicing, nuclear export, and decay [16–19]. One mechanism for these functions is the recognition of m^{6}A by reader proteins. Several m^{6}A readers identified to date contain a YT521-B homology (YTH) domain that specifically binds m^{6}A in an aromatic cage [20–22]. Recently, the nuclear protein heterogeneous ribonucleoprotein C (HNRNPC) was identified as an m^{6}A reader that lacks a YTH domain. Instead, the recognition of m^{6}A by HNRNPC depends on an m^{6}A-induced change in RNA structure [19]. While m^{6}A is capable of Watson-Crick base pairing, thermal denaturation studies with model RNA duplexes have demonstrated that m^{6}A in a duplex is destabilizing by 0.5–1.7 kcal/mol [23,24]. To allow hydrogen bonding at the Watson-Crick face, the *N6*-methyl is rotated such that it is in the *anti* position relative to the N1 across the C6–N6 bond

[23]. The destabilization of the duplex by m^{6}A methylation is likely due to the steric clash between N7 and the *anti N6*-methyl in base-paired m^{6}A [23]. Since HNRNPC binds single-stranded U-tract motifs, methylation of an adenosine in a hairpin-stem can destabilize the duplex to expose an HNRNPC binding site [25,26]. This 'm^{6}A-switch' mechanism was found to be the basis by which HNRNPC recognizes m^{6}A modification at a site in the human lncRNA MALAT1. Further examination of HNRNPC-bound RNAs revealed 2,798 high-confidence m^{6}A-switches in which HNRNPC is thought to use a similar mechanism of indirect m^{6}A recognition [19]. Likewise, other mRNA/lncRNA binding proteins could recognize m^{6}A indirectly via m^{6}A-induced changes in the availability of their structured or single-stranded binding sites. m^{6}A-switch-like RNAs could thus represent a widespread mechanism of m^{6}A function in the cell.

Dynamic RNA structures have extensive roles in the function of structural and regulatory lncRNAs, and in the regulation of mRNA transcription, splicing, translation, and stability [27]. Thus, the effect of m^{6}A on lncRNA and mRNA structure has the potential to influence many cellular processes. *In vitro* studies with model m^{6}A duplexes have demonstrated that m^{6}A can either stabilize or destabilize RNA secondary structures depending on its position within or at the end of a duplex [23]. Further evidence suggests that m^{6}A influences RNA structure *in vivo*. Parallel analysis of RNA structure (PARS) showed that RRACH motifs containing m^{6}A have a different RNA structural profile than RRACH motifs lacking m^{6}A modification [23]. Moreover, structural probing in an *in vivo* click selective 2'-hydroxyl acylation and profiling experiment (icSHAPE) revealed a METTL3-dependent enhancement in reactivity at m^{6}A sites [28]. The widespread influence of m^{6}A on RNA secondary structure in cells could potentially have important consequences for the processing, function, and fate of mRNAs and lncRNAs.

The discovery that an m^{6}A-switch regulates HNRNPC binding revealed that m^{6}A-induced changes in mRNA and lncRNA structure have functional effects *in vivo*. In this study, we further characterized the m^{6}A-induced structural changes in a 32-nucleotide hairpin derived from the m^{6}A-switch in the human lncRNA MALAT1. Nuclear magnetic resonance (NMR) revealed that while the methylated hairpin maintains its overall structure, m^{6}A affects the distances between protons in the hairpin region where m^{6}A is located. Förster resonance energy transfer (FRET) studies further demonstrated that m^{6}A alters the conformation of the MALAT1 hairpin to become more similar to the HNRNPC-bound hairpin, whereas HNRNPC binding induces similar conformations of both the methylated and unmethylated hairpins. Comparing A and m^{6}A hairpins shows that m^{6}A modification predisposes the RNA conformation to resemble more closely its conformation in the RNA–HNRNPC complex.

Results

In previous studies, HNRNPC was found to preferentially bind an m^{6}A-modified hairpin composed of nucleotides 2556–2587 of the lncRNA MALAT1, with an ~8-fold higher affinity for the methylated hairpin [19]. Since HNRNPC is known to recognize single-stranded U-tracts of at least 5 U's in length, it was hypothesized that methylation of A2577 destabilizes the hairpin-stem, exposing the single-stranded U-tract for HNRNPC binding

(Figure 1) [19,25,26]. Structural probing with RNase V1 and S1 nuclease was consistent with this m^{6}A-switch model, showing decreased stacking and increased single-strandedness in the region of the hairpin-stem surrounding A2577 upon m^{6}A modification [19,29]. However, it was not known how extensive the global structural and dynamic differences are between the unmodified and m^{6}A-modified hairpins, and how m^{6}A modification enhances HNRNPC binding to the MALAT1 hairpin. We address these questions here using NMR and FRET methods.

NMR shows that methylation of the MALAT1 hairpin changes the conformation of a portion of the hairpin stem

To examine the differences between the methylated and unmethylated MALAT1 hairpin in solution, we collected 1D ^{1}H NMR spectra of both hairpins at 20 °C in 10% D_2O (Figures 2a–c). Native gel electrophoresis demonstrated that the hairpins migrate as a single major species with the same mobility regardless of methylation status (Figure 2b). The 1D spectra of the two hairpins are largely similar, suggesting that the overall structure of the hairpin is maintained. In particular, the 9.5–14.8 ppm regions show that the chemical shifts of the imino protons H1 and H3 of G and U, respectively, are largely unaffected by methylation of the hairpin (Figure 2c).

We performed 2D nuclear Overhauser effect spectroscopy (NOESY) experiments of the methylated and unmethylated MALAT1 hairpins at 4 °C and 20 °C in 10% D_2O to assign the imino protons and to detect differences in inter-proton distances (Figure 3a–b and Table 1). Sequential NOEs between imino protons of neighboring guanosines and uridines were used for imino proton assignments. Many of the same imino–imino NOEs were present in both methylated and unmethylated hairpins, suggesting that these base–base interactions are maintained and the overall structure of the hairpin does not change upon m^{6}A modification. However, two imino–imino NOEs were observed at 20 °C in the unmethylated hairpin, but not in the methylated hairpin: an NOE between the imino protons of U11 and G21, and an NOE between the imino protons of G9 and U10. Both NOEs involve bases within the U-tract that consists of the binding site for HNRNPC protein. The loss of these NOEs suggests a change in conformation in the upper part of the MALAT1 hairpin-stem. Since NOEs are an indicator of through-space distance, where NOE signal falls rapidly with distance r as $1/r^6$, the loss of the NOE between U11 and G21 imino protons in particular is consistent with the model that this portion of the stem is less stably base paired in the methylated hairpin.

In addition, the methylated hairpin exhibited several changes in the amino–imino region of the NOESY spectrum (Figure 3c). The most pronounced changes were found in NOEs between amino region protons and the imino proton of U10. These amino region resonances likely correspond to protons from the A/m^{6}A22 that base pairs with U10. Similar to previous NMR studies with model m^{6}A duplexes, we observed NOEs of the m^{6}A22 H2 and H6 with the imino proton of the base-paired U10 [23]. Two NOEs were observed between the m^{6}A22 H6 and the imino proton of U10, suggesting slow exchange between the *anti* and *syn* conformations of the *N6* methyl group. The NOEs of the U10 imino proton with the m^{6}A22 H6 proton were stronger than those with the A22 H6a and H6b protons of the

unmethylated hairpin, likely due to slower rotation of the *N6* methylamino group, as has been previously proposed [23]. The NOE between the U10 imino and the A/m^{6}A22 H2 was equally intense in the methylated and unmethylated hairpins, suggesting that the hydrogen bond between the U10 imino proton and m^{6}A22 N1 is retained. Given that the single m^{6}A22 H6 proton shows two NOEs with the U10 imino proton, the m^{6}A-U base pair could be either singly or doubly hydrogen bonded within the hairpin depending on the *syn* or *anti* conformation of the *N6* methyl group in m^{6}A. Previous studies with model m^{6}A duplexes found only one NOE between the m^{6}A H6 and the U imino [23]. This discrepancy is consistent with previous observations that the effect of m^{6}A on stability is strongly context dependent [23,24]. The m^{6}A-U was two G-C pairs from the end of the model m^{6}A duplex used for NMR studies by Roost *et al*. [23], whereas in the MALAT1 hairpin the m^{6}A-U is two G-U pairs from the loop, which could afford more flexibility for the *N6*-methylamino group to rotate.

We further collected 2D NOESY spectra of the methylated and unmethylated MALAT1 hairpins at 20 °C in 100% D_2O (Figure 3d). The resonances were broad and overlapping, such that the intra- and inter-nucleotide H6/H8–H1′ NOEs along the duplex could not be traced unambiguously. Nonetheless, a comparison between the NOESY spectra of the methylated and unmethylated hairpins showed that the H6/H8–H1′ regions were mostly similar, but with several distinct shifts in resonances. These shifted resonances most likely correspond to protons of the m^{6}A22-U10 base pair or of nearby nucleotides. Similar shifts in resonances have been observed in studies with model m^{6}A duplexes [23].

FRET shows that the methylated and unmethylated hairpins have different conformations

To further probe the influence of m^{6}A on the conformation of the MALAT1 hairpin in solution, we designed two pairs of unmethylated and methylated MALAT1 hairpins modified with a 5′ indocarbocyanine-3 (Cy3) fluorophore and an internal fluorescein fluorophore in the hairpin stem (Figure 4a–b). The constructs were named based on the position of the fluorescein fluorophore: the unmethylated and methylated hairpins Fl-8-A and Fl-8-m^{6}A contain fluorescein-dT at nucleotide position 8, while the unmethylated and methylated hairpins Fl-26-A and Fl-26-m^{6}A contain fluorescein-dT at nucleotide position 26.

We observed that m^{6}A modification resulted in a significant increase in FRET efficiency at ambient temperature (Figure 4a–c). In contrast, the methylated and unmethylated hairpins had similar FRET efficiencies when denatured at 90 °C (Figure 4d). Based on these results, we suggest that m^{6}A increases the FRET efficiency by altering the conformation of the MALAT1 hairpin, whereas m^{6}A does not alter the conformation of the unfolded oligo. Changes in FRET efficiency could be due to changes in the distance between donor and acceptor fluorophores or to changes in the relative orientation of the fluorophores. Since the fluorescein donor fluorophore was in the stem of the MALAT1 hairpin, increased flexibility of the hairpin-stem upon m^{6}A modification could alter the position or orientation of the fluorescein fluorophore to increase the efficiency of energy transfer to Cy3 at the 5′ end of the hairpin. This interpretation of the observed FRET efficiencies is consistent with the

m^{6}A-switch model for the MALAT1 hairpin, in which m^{6}A modification increases the flexibility of the hairpin-stem and exposes single-stranded RNA for protein binding.

FRET shows that the conformation of the methylated hairpin is more similar to the HNRNPC-bound RNA conformation

The above results demonstrate that m^{6}A modification of the MALAT1 hairpin changes the conformation of the RNA alone. To evaluate the influence of m^{6}A modification on the conformation of the HNRNPC-bound hairpin, we added HNRNPC protein to the MALAT1 hairpin constructs and measured the resulting FRET spectra. The FRET efficiencies of the methylated and unmethylated MALAT1 hairpins became more similar upon addition of HNRNPC (Figure 5a–b), whereas the FRET efficiencies did not change upon addition of Proteinase K as a control protein (Figure 5c). Thus, although m^{6}A modification alters the conformation of the MALAT1 hairpin alone, in the ribonucleoprotein (RNP) complex the RNA has the same conformation regardless of modification status. We suggest that the difference in the affinity of HNRNPC for the methylated and unmethylated hairpins is the result of a difference in the conformation of the unbound RNA hairpins, whereas the ribonucleoproteins have the same conformation and energetics regardless of RNA methylation. The 8-fold difference in the K_d for HNRNPC binding can be accounted for by a ~1.2 kcal/mol destabilization of the hairpin duplex by m^{6}A to expose the U-tract for HNRNPC binding, consistent with the previously observed 0.5–1.7 kcal/mol destabilizing effect of m^{6}A on model RNA duplexes [23]. The change in the stability of the RNA hairpin explains how formation of an RNP with the methylated hairpin is more thermodynamically favorable than formation of an RNP with the unmethylated hairpin, even though the methylated and unmethylated RNPs are similar in conformation and energy.

For both sets of constructs, the change in FRET efficiency upon protein binding was more drastic for the unmethylated hairpin than for the methylated hairpin (Figure 5c), suggesting that the conformation of the methylated hairpin is more similar to that of the HNRNPC-bound hairpin. Since the conformations of the free and bound m^{6}A-modified hairpin are similar, the conformational change in the conversion of the free form to the bound form might require less energy than the conversion of the unmodified hairpin from the free conformation to the bound conformation. In this manner, m^{6}A modification seems to set up the hairpin for HNRNPC binding by inducing a conformation more similar to the protein-bound form.

Structural modeling shows how m^{6}A can alter the conformation of the MALAT1 hairpin

Using the RNA tertiary structure prediction program MC-Sym [30], we generated 9,999 models for the MALAT1 hairpin and selected models corresponding to the methylated and unmethylated hairpins based on four simultaneous criteria: (1) best fit to the FRET data, (2) best fit to the 2D NOESY data collected with 100 ms mixing time in 10% D_2O, (3) best P-Scores, and (4) maximization of relative FRET yields. While MC-Sym can use NMR data to guide model generation, FRET data involve pairs of models, so they are not amenable to interpretation during model generation. Instead of generating models based on the experimental data, we first generated a large pool of models, then chose those that satisfy all

the data. True conformational sampling would require the use of molecular dynamics simulations, but due to very slow RNA dynamics, this approach is not attempted here.

The selected models were narrowed down to 25 models corresponding to the unmethylated hairpin and 25 models corresponding to the methylated hairpin. The parameters used to calculate the theoretical FRET efficiencies (the orientation parameter κ^2 and the distance between fluorophores) are plotted in Figure 6a. While the distribution of distances is similar for both the "A" and "m^{6}A" sets, the models corresponding to the methylated hairpin ("m^{6}A" set) show more variation in the orientation parameter κ^2. Since the position of the Cy3 fluorophore was kept invariant in all 9,999 models, κ^2 depends primarily on the position and orientation of the fluorescein fluorophore in the hairpin stem. The observation that the "m^{6}A" set shows more variation in κ^2 implies that a wider range of different fluorescein fluorophore orientations is consistent with the FRET and NMR data, raising the possibility that the bases in the stem of the methylated hairpin have greater dynamic flexibility or can adopt multiple distinct conformations.

The centroid of the 25 models was used to generate a single model each for methylated and unmethylated MALAT1 hairpins (Figure 6b). The superimposed model structures reveal an m^{6}A methylation-dependent change in the conformation of the upper stem and loop of the MALAT1 hairpin, including the backbone and nucleobases of the U-tract bound by HNRNPC. Thus, m^{6}A methylation of the hairpin induces a conformational change that propagates through the hairpin structure sufficiently to influence the structure of the HNRNPC binding site, which supports the model that the effect of m^{6}A on the hairpin structure indirectly causes a change in the HNRNPC binding affinity.

Discussion

In this study, we used biophysical methods and modeling to examine the effect of m^{6}A modification on the MALAT1 hairpin. Our NMR and FRET results demonstrate that the general structure of the MALAT1 hairpin is maintained, but the nucleobases of the hairpin-stem are more flexible and solvent accessible upon m^{6}A modification. These results support the m^{6}A-switch model, in which m^{6}A regulates protein binding through its influence on RNA structure [19].

While previous studies examined the influence of m^{6}A on the structure and stability of model RNA duplexes, no past studies used NMR to investigate a physiological m^{6}A-modified RNA [23,24]. The study of nucleic acids by NMR is already challenging due to low proton density and high spectral overlap [32,33]. The terminal loop, internal loop, and noncanonical G-U pairs of the MALAT1 hairpin further complicate the detection and assignment of imino protons by reducing the number of detectable protons, interrupting the continuity of the stem, and introducing ambiguity in the assignment of imino–imino NOEs. The possibility of dynamic changes in structure, base pairing, and oligomerization state introduces additional difficulties in the study of a naturally occurring RNA hairpin. In the future, structural studies of physiological m^{6}A-modified RNA might take advantage of selective labeling with ^{15}N or ^{13}C isotopes. Such methods would enable direct observation

of hydrogen bonding, unambiguous identification of noncanonical base–base interactions, and better resolution of local changes in conformation [32,33].

The FRET constructs used in this study showed that m^{6}A modification influences the observed FRET efficiency, likely due to an m^{6}A-induced change in the conformation of the MALAT1 hairpin. However, ensemble FRET studies cannot distinguish a homogeneous population adopting a single conformation from a heterogeneous population with multiple subpopulations or with dynamically changing conformations [34]. It is very possible that the m^{6}A-modified hairpins not only have a different average structure, but are also more dynamic or adopt a more heterogeneous set of different conformations. It would be very interesting to study our constructs using single-molecule FRET in order to better understand how m^{6}A influences the conformational dynamics of the MALAT1 hairpin. Single-molecule FRET studies are well-suited to studying dynamic systems and have provided insight into processes such as RNA folding and RNP formation [35]. In addition to clarifying the structure and dynamics of the MALAT1 hairpin, single-molecule FRET could further elucidate how m^{6}A affects hairpin folding and protein binding.

The MALAT1 hairpin is the first identified example of an m^{6}A-switch, but the changes induced by m^{6}A modification of the MALAT1 hairpin are likely generalizable to a much larger family of m^{6}A-regulated RNA structures. Over 2,000 high-confidence m^{6}A-switches have been identified at HNRNPC binding sites [19]. In addition, the m^{6}A-switch mechanism has the potential to regulate the binding of other RNA binding proteins through altered accessibility of their single-stranded RNA binding motifs or through changes in their cognate RNA structures. Thus far, the only m^{6}A reader proteins known to directly bind m^{6}A belong to the YTH family of proteins [18]. While other direct m^{6}A binders might yet be discovered, the m^{6}A-switch mechanism expands the pool of candidate m^{6}A readers to a much wider array of RNA binding proteins. Indirect m^{6}A readers might be pervasive but difficult to discover because in many cases only a subset of their targets might be regulated by m^{6}A modification. For example, m^{6}A-switches seem to regulate ~8% or ~40,000 of all known HNRNPC binding sites [19]. Moving forward, it will be important to investigate other indirect m^{6}A readers and the mechanisms by which m^{6}A alters RNA structure to influence protein binding.

As the most abundant post-transcriptional modification in eukaryotic mRNA and lncRNA, m^{6}A could have pervasive regulatory roles in the regulation of mRNA transcription, splicing, and translation, and in influencing the structure and function of lncRNAs. In addition, m^{6}A modification might influence RNA structures in other classes of noncoding RNA. For example, m^{6}A methylation of primary microRNAs (pri-miRNAs) has recently been shown to be crucial for recognition by the microprocessor complex, though it is unclear in this case whether m^{6}A functions by influencing RNA structure or through direct recognition [36]. While m^{6}A modification likely regulates many m^{6}A-switches using the same mechanism as in the MALAT1 hairpin, m^{6}A could potentially use other mechanisms to regulate RNA structures such as disrupting a tertiary hydrogen bond [7]. Even in an RNA stem-loop, the influence of m^{6}A on RNA structure is dependent on context, as m^{6}A can either stabilize or destabilize depending on its position. It will be important to investigate the diverse and context-dependent effects of m^{6}A on RNA structure and dynamics, and how

these are linked to the functions of m^6A in the cell. As the first example of an m^6A-induced structural change in a cellular RNA, the MALAT1 m^6A-switch is an initial model for a potentially much more general mechanism by which m^6A achieves its functions in the cell.

Materials and Methods

RNA synthesis and purification

RNA oligos containing two fluorophore modifications in each sequence were synthesized by Expedite DNA synthesizer on a 1 μmol scale. Cy3 phosphoramidite and fluorescein-dT phosphoramidite were purchased from Glen Research. m^6A phosphoramidite was prepared by following our reported procedure [37]. All the other phosphoramidites and beads were purchased from Chemgene. After oligo synthesis, the RNA oligos were first deprotected by treatment with 30% ammonium hydroxide and ethanol (3:1, v/v) at 55 °C for 4 h. Once cooled to ambient temperature, the supernatant was dried in a SpeedVac and the resulting pellets were further deprotected by treatment with a mixture of dimethyl sulfoxide (100 μL) and hydrogen fluoride triethylamine (125 μL) at 65 °C for 2.5 h. After cooling to ambient temperature, 22.5 μL sodium acetate (3 M) and *n*-butanol (1 mL) were added, and the mixture was vortexed and precipitated at −80 °C for 1 h. After centrifugation, the supernatant was removed, and the pellets were washed with 70% ethanol and purified on an 8% acrylamide:bisacrylamide (29:1), 7 M urea, 89 mM Tris Borate pH 8.3, 2 mM Na_2EDTA gel. RNA was excised from the gel by UV shadowing and eluted in 50 mM potassium acetate, 200 mM KCl, pH 7.5 by the crush-and-soak method. Eluted RNA was precipitated in ethanol, then resuspended and stored in H_2O at −20 °C.

RNA oligos M2577-A and M2577-m^6A were synthesized, deprotected, and purified in a similar way except that we used a Mermade synthesizer on a 5 μmol scale.

HNRNPC protein expression and purification

Rosetta BL21 *Escherichia coli* were transformed with a pGEX-6P-1 plasmid containing the full-length HNRNPC1 coding sequence inserted between the BamHI and XhoI restriction sites. The transformed bacteria were grown to saturation at 37 °C, 200 rpm in Luria–Bertani Lennox media with 100 μg/mL ampicillin and 50 μg/mL chloramphenicol, then diluted 1:100, grown in the same culture media to an absorbance of ~0.6 at 600 nm, and induced with 2.5 mM isopropyl β-D-1-thiogalactoside (IPTG). The bacteria were grown an additional 5 hours at 37 °C, 200 rpm, then harvested and sonicated at 4 °C. GST–HNRNPC1 fusion protein was isolated from the soluble lysate using GST•Bind resin (Novagen), and then cleaved by GST-tagged PreScission Protease for 16 hours at 4 °C. The purified full-length HNRNPC1 protein was stored in 10 mM Tris pH 7.5, 100 mM KCl, 2.5 mM $MgCl_2$, 30% glycerol (v/v) at −80 °C.

NMR spectroscopy

NMR data were acquired on a Bruker AVANCE III 600 MHz (14 Tesla) NMR spectrometer with a 5 mm pulsed field gradient (z-axis) triple HCN probe, and were processed using TopSpin v3.2 software. All NMR experiments were conducted at 20 °C, with trimethylsilyl propanoic acid (TSP) as the ^1H chemical shift reference. Gel-purified RNA in H_2O was

centrifuged 10 minutes at 17K·*g* to sediment any particulate matter. The supernatant RNA was combined with Na_2HPO_4 buffer at pH 7.4 and incubated 1 minute at 90 °C, then 3 minutes at ambient temperature. $MgCl_2$, D_2O, and TSP were added to a final volume of 500 μL with 10 mM Na_2HPO_4 pH 7.4, 2.5 mM $MgCl_2$, 90% H_2O / 10% D_2O (v/v). The samples were then incubated 5 minutes at ambient temperature and stored at 4 °C until data collection. 1D ^1H NMR spectra of the RNA hairpins were collected at 1.12 mM concentration, with 1028 scans. 2D ^1H NOESY spectra in 90% H_2O / 10% D_2O (v/v) were acquired with 100 ms mixing time, with 256 scans. 2048 points were taken in F2 and 512 points in F1, with a recycle delay of 1 second and a spectral width of 22 ppm in both dimensions. The RNA concentration was 1.12 mM for the 2D NOESY scans at 20 °C, and 0.47 mM for the 2D NOESY scans at 4 °C. 2D ^1H NOESY spectra of 0.78 mM RNA in 100% D_2O were acquired with 100 ms mixing time, with 256 scans. 2048 points were taken in F2 and 512 points in F1, with a recycle delay of 1 second and a spectral width of 9 ppm in both dimensions.

FRET experiments

FRET spectra were acquired on a HORIBA FluoroLog-3 Spectrofluorometer equipped with a Peltier controller, and processed using FluorEssence v3.5 software. 1 μM gel-purified RNA in H_2O was combined with Tris pH 7.5 buffer and incubated 2 minutes at 90 °C, then 3 minutes at ambient temperature. KCl and $MgCl_2$ were added to a final volume of 100 μL with conditions 500 nM RNA, 10 mM Tris pH 7.5, 100 mM KCl, 2.5 mM $MgCl_2$. For experiments with protein binding, HNRNPC was added with the same final buffer conditions. For experiments with denatured RNA, the sample was incubated at least 5 minutes at 90 °C, and the spectra were measured with the Peltier controller set at 90 °C. The samples were transferred to the cuvette and emission spectra were collected from 500 nm to 750 nm using the excitation wavelength 490 nm, with excitation and emission spectral slit widths of 2 nm and 5 nm, respectively. A buffer solution of 10 mM Tris pH 7.5, 100 mM KCl, 2.5 mM $MgCl_2$ was used as the emission spectrum blank. FRET efficiencies were calculated as $E_{FRET,relative} = I_A/(I_D+I_A)$, where I_D is the emission intensity at 518 nm and I_A is the emission intensity at 563 nm.

Structural modeling

The 33-nucleotide sequence 5′-UAACUUAAUGUUUUUGCAUUGGACUUUGAGUUA with secondary structure “(((((((.((((…….)))).)))))))”, where parentheses denote base pairs and dots denote non-base-paired residues, was used to generate 910 decoy RNA tertiary structures. The decoys varied from one another only in the U0–A32 base pair, where the 5′-most nucleobase U0 was added as a placeholder for the Cy3 fluorophore present in the FRET oligos. Each of the 910 decoys was used to generate 9,999 RNA tertiary structure models for the MALAT1 hairpin using the MC-Sym computer program. Within each decoy set, the U0–A32 and A1–U31 base pairs were invariant. The decoy set that generated the most pairs that fit the FRET data for either Fl-8-A/m^6A or Fl-26-A/m^6A was used to select models for the methylated and unmethylated hairpins. Rather than assigning weights to the various experimental parameters, we used the experimental data as filters in a sequential fashion, and the final selected models do not depend on the order of application of the filters.

Models were selected from the 9,999 structural models in the decoy set based on four simultaneous criteria: (1) best fit to the FRET data, (2) best fit to the 2D NOESY data, (3) best P-Scores, and (4) maximization of relative FRET yields.

(1) Best fit to the FRET data—The theoretical FRET efficiencies were calculated as

$$\mathrm{E}_{\mathrm{FRET,rel}}=\frac{1}{1+(R^6/{R_0}^6)}$$

with

$${R_0}^6=(55.7\text{Å})^6\cdot\kappa^2\cdot{}^3\!/_2$$

and

$$\kappa=\mathbf{D}\cdot\mathbf{A}-3(\mathbf{R}\cdot\mathbf{D})(\mathbf{R}\cdot\mathbf{A})$$

where **D** and **A** are the unit vectors oriented from N1 to C4 of the uridine nucleotides corresponding to the donor and acceptor fluorophores, respectively, **R** is the unit vector oriented from the donor position H3 to the acceptor position H3, and *R* is the distance from the donor H3 to the acceptor H3. Only pairs of structures for which the theoretical E_{FRET}(A) / E_{FRET}(m^6A) ratios were within 0.01 of the experimental ratios for Fl-8-A/m^6A and Fl-26-A/m^6A were kept (122,844 A–m^6A pairs).

(2) Best fit to the 2D NOESY data—To extract inter-proton distance information from the 2D NOESY data at 20 °C in 10% D_2O with 100 ms mixing time, we assumed a linear relationship between peak intensity and mixing time:

$$\eta=2W_\mathrm{o}t_\mathrm{mix}$$

where η is the NOE peak intensity, W_o is the rate of the zero-quantum transition, and t_{mix} is the mixing time (100 ms). Using this approximation, the inter-proton distance *r* is related to the peak intensity by

$$r^6\propto\frac{1}{W_\mathrm{o}}\propto\frac{1}{\eta}$$

so the experimental NOE intensities and the relative distances between imino protons in the modeled tertiary structures were used to calculate log(r_x^6 / r_o^6) ratios, where r_x is the inter-proton distance for a pair of imino protons, and r_o is the distance between G27 H1 and U5 H3. The least squares differences between the five experimental and modeled log(r_x^6 / r_o^6) ratios were then used to classify the modeled structures as either “A” or “m^6A” depending on whether they were a closer fit to the unmethylated or methylated hairpin, respectively. Using this method, 8,176 structures were assigned as “A,” while 1,823 were assigned as

"m^6A." Only pairs of structures for which the "A" and "m^6A" assignments were consistent with the assignments based on the FRET efficiencies were kept.

(3) The P-Score—for each modeled RNA tertiary structure was calculated based on the phosphate chain torsion angles in the predicted tertiary structures as described previously [31]. P-scores involve as many as four consecutive phosphate groups, and their aim is to assess how natural the modeled RNA looks like given the backbone trace. Only the top 5,000 of the 9,999 tertiary structures in the decoy set were kept.

(4) Maximization of relative FRET yields—Once the original 9,999 structures in the decoy set were filtered based on their FRET fit, NOE fit, and P-Scores, there were 276 remaining structures corresponding to the unmethylated hairpin, and 713 structures corresponding to the methylated hairpin. These were narrowed down to 25 models each corresponding to the unmethylated and methylated hairpins by maximizing the density of A–m^6A pairs. To achieve density maximization, a structural model that has been selected to be a representative of the "A" state (Figure 6a, gray dots) must maximize the number of structural models in the "m^6A" state (Figure 6a, dark red dots) for which the relative FRET efficiency yielded is close to the one experimentally observed (gray lines connecting the dots). The same principle was applied while populating the "m^6A" state; models must maximize the number of "A" state relative FRET yields.

Acknowledgments

This work was supported by the NIH (DP1GM105386, R01GM113194 to T.P., K01HG006699 to Q.D.) and the NIH Medical Scientist Training Program grant NIGMS T32GM007281 (K.I.Z.). The authors would like to thank the generous support of the University of Chicago Biological Sciences Division and the Frank Family Endowment (K.I.Z.).

References

1. Carlile TM, Rojas-Duran MF, Zinshteyn B, Shin H, Bartoli KM, Gilbert WV. Pseudouridine profiling reveals regulated mRNA pseudouridylation in yeast and human cells. Nature. 2014; 515:143–146. [PubMed: 25192136]
2. Desrosiers R, Friderici K, Rottman F. Identification of methylated nucleosides in messenger RNA from Novikoff hepatoma cells. Proc Natl Acad Sci. 1974; 71:3971–3975. [PubMed: 4372599]
3. Dominissini D, Moshitch-Moshkovitz S, Schwartz S, Salmon-Divon M, Ungar L, Osenberg S, et al. Topology of the human and mouse m6A RNA methylomes revealed by m6A-seq. Nature. 2012; 485:201–206. [PubMed: 22575960]
4. Meyer KD, Saletore Y, Zumbo P, Elemento O, Mason CE, Jaffrey SR. Comprehensive Analysis of mRNA Methylation Reveals Enrichment in ′ UT s and near Stop Codons. Cell. 2012; 149:1635–1646. [PubMed: 22608085]
5. Squires JE, Patel HR, Nousch M, Sibbritt T, Humphreys DT, Parker BJ, et al. Widespread occurrence of 5-methylcytosine in human coding and non-coding RNA. Nucleic Acids Res. 2012; 40:5023–5033. [PubMed: 22344696]
6. Schwartz S, Agarwala SD, Mumbach MR, Jovanovic M, Mertins P, Shishkin A, et al. High-Resolution Mapping Reveals a Conserved, Widespread, Dynamic mRNA Methylation Program in Yeast Meiosis. Cell. 2013; 155:1409–1421. [PubMed: 24269006]
7. Pan T. N6-methyl-adenosine modification in messenger and long non-coding RNA. Trends Biochem Sci. 2013; 38:204–209. [PubMed: 23337769]

8. Liu J, Yue Y, Han D, Wang X, Fu Y, Zhang L, et al. A METTL3–METTL14 complex mediates mammalian nuclear RNA N6-adenosine methylation. Nat Chem Biol. 2013; 10:93–95. [PubMed: 24316715]
9. Ping X-L, Sun B-F, Wang L, Xiao W, Yang X, Wang W-J, et al. Mammalian WTAP is a regulatory subunit of the RNA N6-methyladenosine methyltransferase. Cell Res. 2014; 24:177–189. [PubMed: 24407421]
10. Zheng G, Dahl JA, Niu Y, Fedorcsak P, Huang C-M, Li CJ, et al. ALKBH5 Is a Mammalian RNA Demethylase that Impacts RNA Metabolism and Mouse Fertility. Mol Cell. 2012
11. Jia G, Fu Y, Zhao X, Dai Q, Zheng G, Yang Y, et al. N6-Methyladenosine in nuclear RNA is a major substrate of the obesity-associated FTO. Nat Chem Biol. 2011; 7:885–887. [PubMed: 22002720]
12. Fustin J-M, Doi M, Yamaguchi Y, Hida H, Nishimura S, Yoshida M, et al. RNA-Methylation-Dependent RNA Processing Controls the Speed of the Circadian Clock. Cell. 2013; 155:793–806. [PubMed: 24209618]
13. Geula S, Moshitch-Moshkovitz S, Dominissini D, Mansour AA, Kol N, Salmon-Divon M, et al. Stem cells. m6A mRNA methylation facilitates resolution of naïve pluripotency toward differentiation. Science. 2015; 347:1002–1006. [PubMed: 25569111]
14. Batista PJ, Molinie B, Wang J, Qu K, Zhang J, Li L, et al. m6A RNA Modification Controls Cell Fate Transition in Mammalian Embryonic Stem Cells. Cell Stem Cell. 2014; 15:707–719. [PubMed: 25456834]
15. Wang Y, Li Y, Toth JI, Petroski MD, Zhang Z, Zhao JC. N6-methyladenosine modification destabilizes developmental regulators in embryonic stem cells. Nat Cell Biol. 2014; 16:191–198. [PubMed: 24394384]
16. Niu Y, Zhao X, Wu Y-S, Li M-M, Wang X-J, Yang Y-G. N6-methyl-adenosine (m6A) in RNA: An Old Modification with A Novel Epigenetic Function. Genomics Proteomics Bioinformatics. 2013; 11:8–17. [PubMed: 23453015]
17. Fu Y, Dominissini D, Rechavi G, He C. Gene expression regulation mediated through reversible m6A RNA methylation. Nat Rev Genet. 2014; 15:293–306. [PubMed: 24662220]
18. Wang X, Lu Z, Gomez A, Hon GC, Yue Y, Han D, et al. N6-methyladenosine-dependent regulation of messenger RNA stability. Nature. 2014; 505:117–120. [PubMed: 24284625]
19. Liu N, Dai Q, Zheng G, He C, Parisien M, Pan T. N6-methyladenosine-dependent RNA structural switches regulate RNA–protein interactions. Nature. 2015; 518:560–564. [PubMed: 25719671]
20. Theler D, Dominguez C, Blatter M, Boudet J, Allain FH-T. Solution structure of the YTH domain in complex with N6-methyladenosine RNA: a reader of methylated RNA. Nucleic Acids Res. 2014; 42:13911–13919. [PubMed: 25389274]
21. Xu C, Wang X, Liu K, Roundtree IA, Tempel W, Li Y, et al. Structural basis for selective binding of m6A RNA by the YTHDC1 YTH domain. Nat Chem Biol. 2014; 10:927–929. [PubMed: 25242552]
22. Luo S, Tong L. Molecular basis for the recognition of methylated adenines in RNA by the eukaryotic YTH domain. Proc Natl Acad Sci. 2014; 111:13834–13839. [PubMed: 25201973]
23. Roost C, Lynch SR, Batista PJ, Qu K, Chang HY, Kool ET. Structure and Thermodynamics of N^6-Methyladenosine in RNA: A Spring-Loaded Base Modification. J Am Chem Soc. 2015; 137:2107–2115. [PubMed: 25611135]
24. Kierzek E. The thermodynamic stability of RNA duplexes and hairpins containing N6-alkyladenosines and 2-methylthio-N6-alkyladenosines. Nucleic Acids Res. 2003; 31:4472–4480. [PubMed: 12888507]
25. Zarnack K, König J, Tajnik M, Martincorena I, Eustermann S, Stévant I, et al. Direct Competition between hnRNP C and U2AF65 Protects the Transcriptome from the Exonization of Alu Elements. Cell. 2013; 152:453–466. [PubMed: 23374342]
26. Cieniková Z, Damberger FF, Hall J, Allain FH-T, Maris C. Structural and Mechanistic Insights into Poly(uridine) Tract Recognition by the hnRNP C RNA Recognition Motif. J Am Chem Soc. 2014; 136:14536–14544. [PubMed: 25216038]
27. Wan Y, Kertesz M, Spitale RC, Segal E, Chang HY. Understanding the transcriptome through RNA structure. Nat Rev Genet. 2011; 12:641–655. [PubMed: 21850044]

28. Spitale RC, Flynn RA, Zhang QC, Crisalli P, Lee B, Jung J-W, et al. Structural imprints in vivo decode RNA regulatory mechanisms. Nature. 2015; 519:486–490. [PubMed: 25799993]
29. Liu N, Parisien M, Dai Q, Zheng G, He C, Pan T. Probing N6-methyladenosine RNA modification status at single nucleotide resolution in mRNA and long noncoding RNA. RNA. 2013; 19:1848–1856. [PubMed: 24141618]
30. Parisien M, Major F. The MC-Fold and MC-Sym pipeline infers RNA structure from sequence data. Nature. 2008; 452:51–55. [PubMed: 18322526]
31. Parisien M, Cruz JA, Westhof E, Major F. New metrics for comparing and assessing discrepancies between RNA 3D structures and models. RNA. 2009; 15:1875–1885. [PubMed: 19710185]
32. Latham MP, Brown DJ, McCallum SA, Pardi A. NMR Methods for Studying the Structure and Dynamics of RNA. Chem Bio Chem. 2005; 6:1492–1505.
33. Zídek L, Stefl R, Sklenár V. NMR methodology for the study of nucleic acids. Curr Opin Struct Biol. 2001; 11:275–281. [PubMed: 11406374]
34. Weiss S. Measuring conformational dynamics of biomolecules by single molecule fluorescence spectroscopy. Nat Struct Mol Biol. 2000; 7:724–729.
35. Alemán EA, Lamichhane R, Rueda D. Exploring RNA folding one molecule at a time. Curr Opin Chem Biol. 2008; 12:647–654. [PubMed: 18845269]
36. Alarcón CR, Lee H, Goodarzi H, Halberg N, Tavazoie SF. N6-methyladenosine marks primary microRNAs for processing. Nature. 2015; 519:482–485. [PubMed: 25799998]
37. Dai Q, Fong R, Saikia M, Stephenson D, Yu Y-t, Pan T, et al. Identification of recognition residues for ligation-based detection and quantitation of pseudouridine and N6-methyladenosine. Nucleic Acids Res. 2007; 35:6322–6329. [PubMed: 17881375]
38. Darty K, Denise A, Ponty Y. VARNA: Interactive drawing and editing of the RNA secondary structure. Bioinformatics. 2009; 25:1974–1975. [PubMed: 19398448]

Highlights

- M^6A alters the conformation of the HNRNPC binding site in a MALAT1 hairpin.
- M^6A modification biases the MALAT1 hairpin toward its protein-bound conformation.
- M^6A can influence many cellular functions by influencing protein binding.

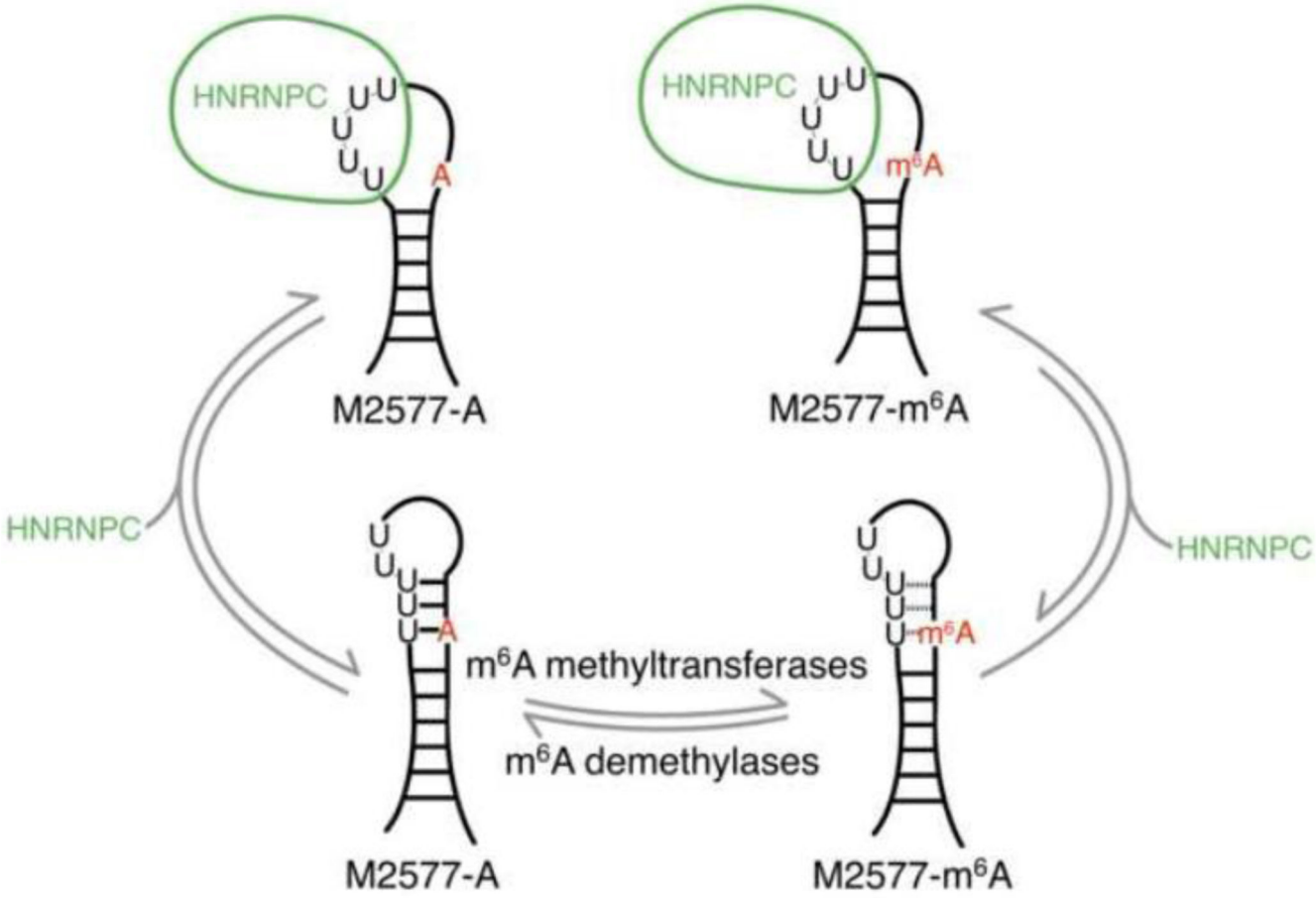

Fig. 1. The m^{6}A-switch model

The human lncRNA MALAT1 is reversibly methylated at position A2577. The protein HNRNPC binds to the U_5-tract in this hairpin from MALAT1, with an ~8-fold higher affinity for the methylated hairpin. One of the U's in the HN NPC binding site pairs with the methylation site A2577. The presence of m^{6}A weakens the base pair and increases the accessibility of the U-tract for protein binding.

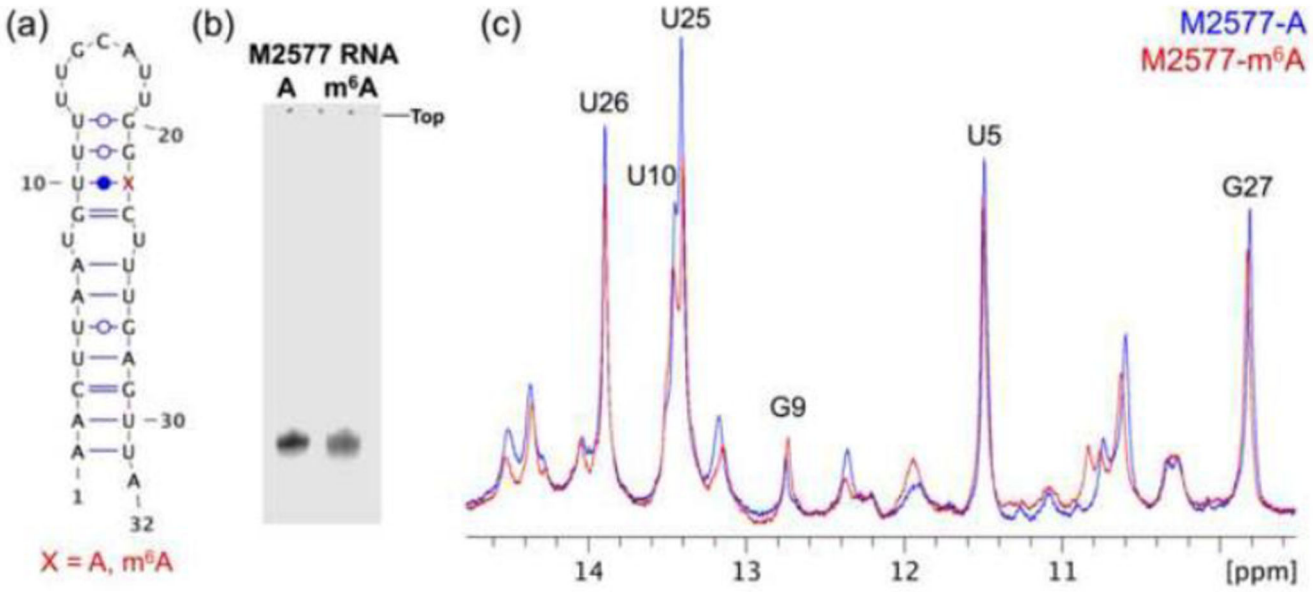

Fig. 2. 1D NMR spectra show that the overall structure of the hairpin is maintained

(a) Secondary structure of the 32-nt M2577-A oligo from nucleotides 2556–2587 of MALAT1. The m^6A modification site (A22 in the oligo, or A2577 in MALAT1) is denoted with a red "X." The figure was made using Visualization Applet for RNA (VARNA) [38]. (b) 15% native PAGE of the unmethylated (M2577-A) and methylated (M2577-m^6A) hairpins in 25 mM Tris acetate pH 7.4, 2.5 mM magnesium acetate. (c) Superimposed imino regions of the 1D ^1H NMR spectra of M2577-A (blue) and M2577-m^6A (red). Watergate solvent suppression 1D ^1H NMR spectra were measured under the conditions 1.12 mM RNA,10 mM Na_2HPO_4 pH 7.4, 2.5 mM $MgCl_2$, 90% H_2O / 10% D_2O (v/v), 20 °C.

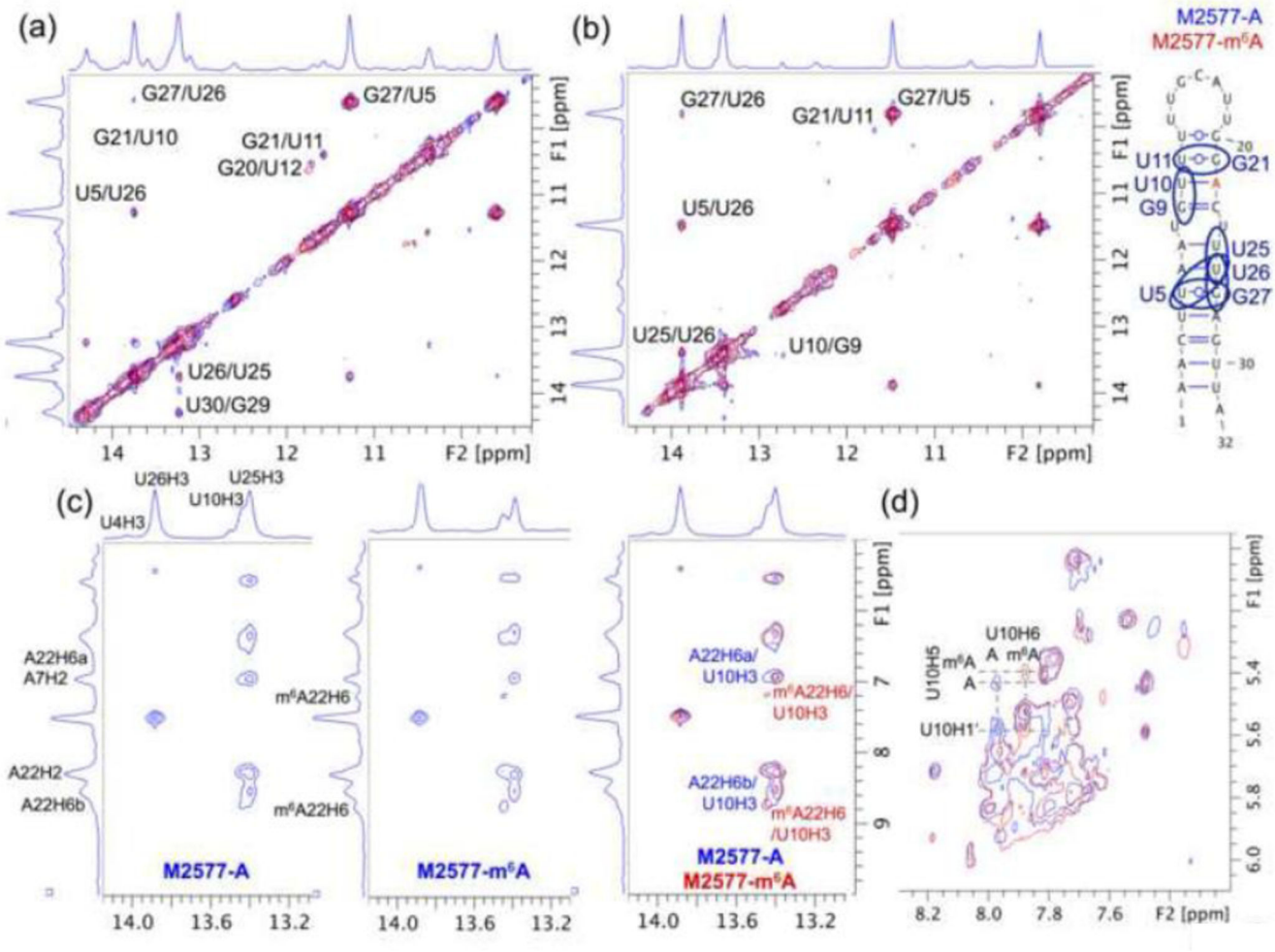

Fig. 3. 2D NOESY spectra show that the upper stem is more dynamic in the methylated than in the unmethylated M2577 hairpin

(a) Superimposed imino regions of the 2D ^{1}H NOESY NMR spectra of M2577-A (blue) and M2577-m^{6}A (red) in 10% D_2O. The spectra of 0.47 mM RNA were measured at 4 °C with a 100 ms mixing time. (b) Superimposed imino regions of the 2D ^{1}H NOESY NMR spectra of M2577-A and M2577-m^{6}A in 10% D_2O. The spectra of 1.12 mM RNA were measured at 20 °C with a 100 ms mixing time. (c) Separate and superimposed amino–imino regions of the 2D ^{1}H NOESY NMR spectra of M2577-A and M2577-m^{6}A in 10% D_2O at 20 °C. (d) Superimposed H6/H8–H1′ regions of the 2D ^{1}H NOESY NMR spectra of M2577-A and M2577-m^{6}A in 100% D_2O. The spectra of 0.78 mM RNA were measured at 20 °C with a 100 ms mixing time.

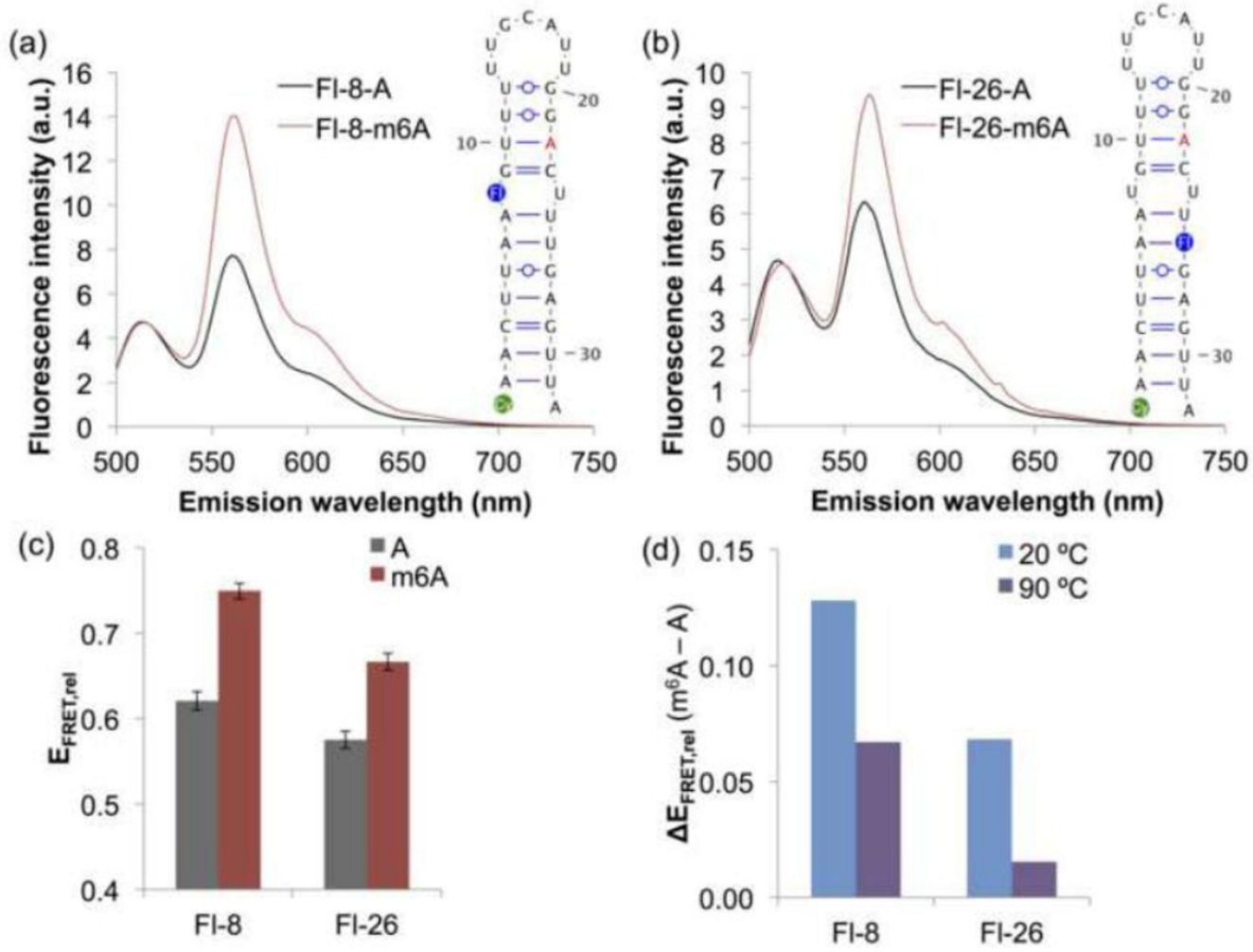

Fig. 4. FRET shows that the methylated and unmethylated MALAT1 hairpins have different conformations

(a) Fluorescence emission spectra of the FRET constructs Fl-8-A and Fl-8-m^{6}A upon excitation at 490 nm. Cy3 (green) is conjugated to the 5′ phosphate, and fluorescein-dT (Fl) is incorporated at the indicated position (blue) in each oligo. Spectra were measured under the conditions 500 nM RNA, 10 mM Tris pH 7.5, 100 mM KCl, 2.5 mM $MgCl_2$ at ambient temperature. Each spectrum is the average of 2–3 measurements. (b) Fluorescence emission spectra of Fl-26-A and Fl-26-m^{6}A upon excitation at 490 nm. (c) Relative FRET efficiencies ($E_{FRET,rel}$) of M2577-A and M2577-m^{6}A, calculated as $I_{563}/(I_{563}+I_{518})$, where I_x is the fluorescence emission intensity at x nm. FRET efficiencies are the mean of 6–8 measurements. Error bars represent ± one standard deviation. (d) Difference in the relative FRET efficiencies of M2577-A and M2577-m^{6}A at ambient temperature (~20 °C) or at 90 °C.

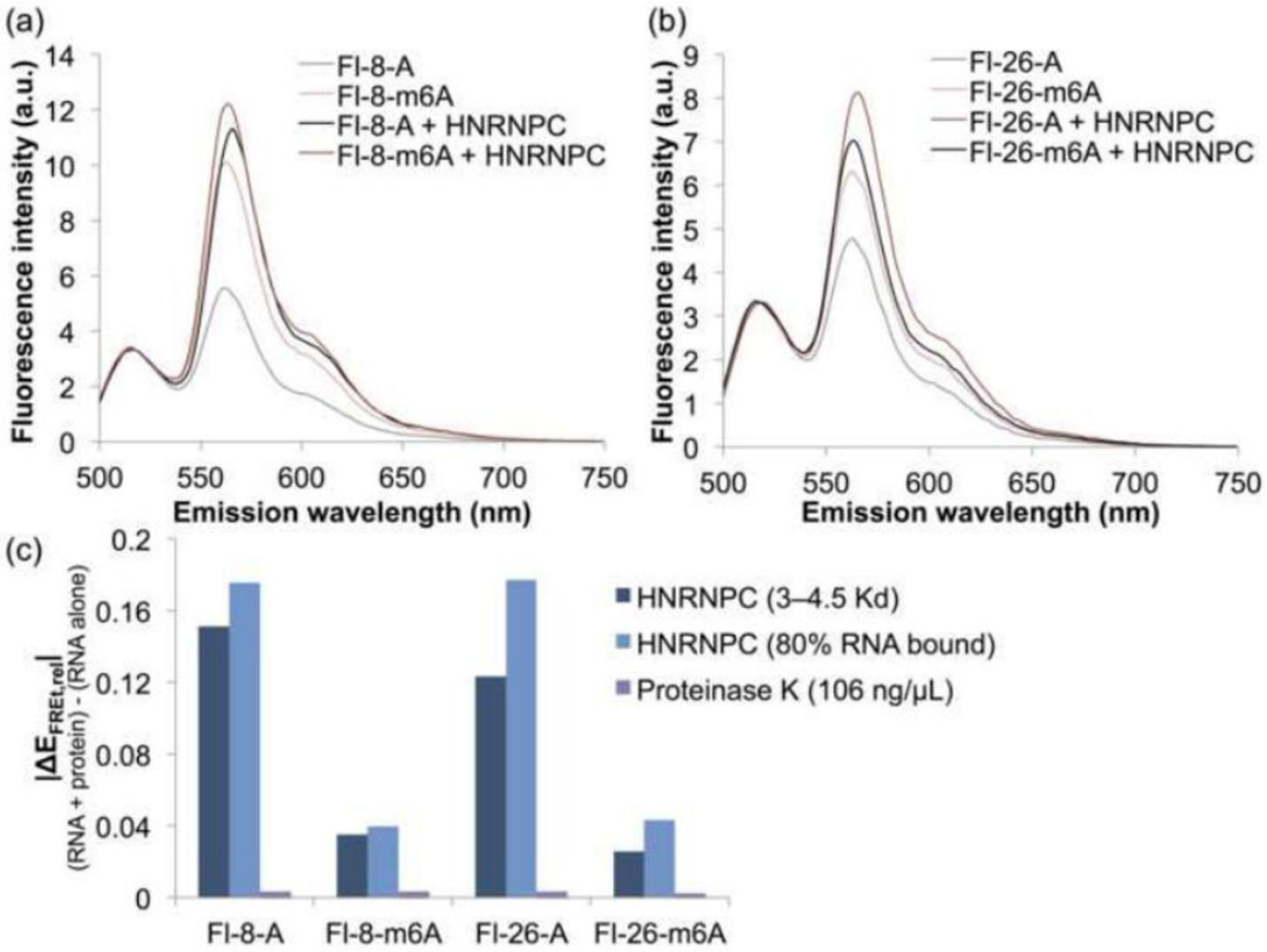

Fig. 5. FRET of RNPs containing the M2577-A and M2577-m^{6}A hairpins

The RNPs show similar FRET, suggesting that the conformation of the RNA in the RNP is the same regardless of the presence of m^{6}A. In addition, the methylated hairpins exhibit a smaller change in FRET upon HNRNPC binding. (a) Fluorescence emission spectra of 500 nM Fl-8-A and Fl-8-m^{6}A with or without addition of HNRNPC at a concentration of 3–4.5·K_d (K_d = 722 nM for M2577-A, K_d = 93 nM for M2577-m^{6}A) [19]. Spectra were measured under the conditions 500 nM RNA, 10 mM Tris pH 7.5, 100 mM KCl, 2.5 mM $MgCl_2$ at ambient temperature at excitation wavelength 490 nm. (b) Fluorescence emission spectra of 500 nM Fl-26-A and Fl-26-m^{6}A with or without addition of HNRNPC at a concentration of 3–4.5·K_d. (c) Change in the relative FRET efficiency ($\Delta E_{FRET,rel}$) of each hairpin (500 nM) upon addition of: 3–4.5·K_d HNRNPC (2.17 μM HNRNPC for M2577-A; 410 nM HNRNPC for M2577-m^{6}A), HNRNPC such that $[RNP]/[RNA]_{total}$ = 80% (3.29 μM HNRNPC for M2577-A; 770 nM HNRNPC for M2577-m^{6}A), or 106 ng/μL Proteinase K (equivalent to weight/volume concentration of 3.25 μM HNRNPC).

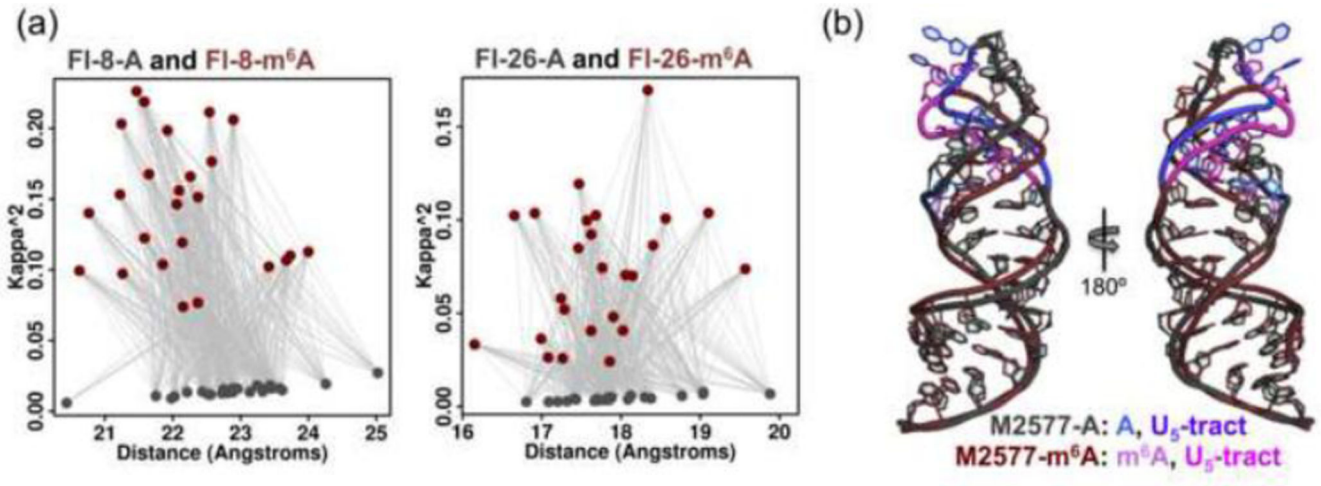

Fig. 6. Structural models for M2577-A and M2577-m^{6}A based on FRET and NMR data

(a) Plot of 25 selected structures for M2577-A (gray) and M2577-m^{6}A (dark red), in terms of κ^2 and distance between fluorophores for Fl-8-A/m^{6}A and Fl-26A/m^{6}A. The structures were selected from an initial set of 9,999 tertiary structures for the M2577 hairpin [30] (c) Structural models of M2577-A (gray) and M2577-m^{6}A (dark red), computed as the centroid of the 25 selected structures. The m^{6}A modification site and the U_5-tract are highlighted in shades of blue for the unmethylated MALAT1 hairpin, and in magenta for the methylated hairpin.

Table 1

Imino–imino NOE intensity in 10% D_2O at 20 °C.

Imino–imino pair	NOE intensity for M2577-A	NOE intensity for M2577-m^6A
G27H1–U5H3	1.00 ± 0.00	1.00 ± 0.00
U5H3–U26H3	0.20 ± 0.02	0.17 ± 0.03
U25H3–U26H3	0.16 ± 0.03	0.18 ± 0.01
G27H1–U26H3	0.06 ± 0.01	0.06 ± 0.00
G21H1–U11H3	0.05 ± 0.02	0.00 ± 0.01
G9H1–U10H3	0.04 ± 0.01	0.01 ± 0.00